The Astrophysical Journal, 787:170 (11pp), 2014 June 1 doi:10.1088/0004-637X/787/2/170

LABORATORY INFRARED SPECTROSCOPY OF GASEOUS NEGATIVELY CHARGED POLYAROMATIC HYDROCARBONS

Juehan Gao[1], Giel Berden[1], and Jos Oomens[1,2]
[1] Radboud University Nijmegen, Institute for Molecules and Materials, FELIX Facility, Toernooiveld 7, 6525-ED Nijmegen, The Netherlands
[2] Van't Hoff Institute for Molecular Sciences, University of Amsterdam, Science Park 904, 1098-XH Amsterdam, The Netherlands; joso@science.ru.nl
Received 2014 March 13; accepted 2014 April 21; published 2014 May 15

ABSTRACT

Based largely on infrared spectroscopic evidence, polycyclic aromatic hydrocarbon (PAH) molecules are now widely accepted to occur abundantly in the interstellar medium. Laboratory infrared spectra have been obtained for a large variety of neutral and cationic PAHs, but data for anionic PAHs are scarce. Nonetheless, in regions with relatively high electron densities and low UV photon fluxes, PAHs have been suggested to occur predominantly as negatively charged ions (anions), having substantial influence on cloud chemistry. While some matrix spectra have been reported for radical anion PAHs, no data is available for even-electron anions, which are more stable against electron detachment. Here we present the first laboratory infrared spectra of deprotonated PAHs ($[PAH - H]^-$) in the wavelength ranges between 6 and 16 μm and around 3 μm. Wavelength-dependent infrared multiple-photon electron detachment is employed to obtain spectra for deprotonated naphthalene, anthracene, and pyrene in the gas phase. Spectra are compared with theoretical spectra computed at the density functional theory level. We show that the relative band intensities in different ranges of the IR spectrum deviate significantly from those of neutral and positively charged PAHs, and moreover from those of radical anion PAHs. These relative band intensities are, however, well reproduced by theory. An analysis of the frontier molecular orbitals of the even- and odd-electron anions reveals a high degree of charge localization in the deprotonated systems, qualitatively explaining the observed differences and suggesting unusually high electric dipole moments for this class of PAH molecules.

Key words: astrochemistry – infrared: ISM – ISM: molecules – methods: laboratory: molecular – molecular data – techniques: spectroscopic

Online-only material: color figures

1. INTRODUCTION

Polycyclic aromatic hydrocarbon (PAH) molecules are now generally considered to be abundantly present in inter- and circumstellar environments and have been linked to different spectroscopic observations (Williams & Taylor 1996), including the UV bump around 220 nm, the diffuse interstellar bands and the infrared emission features, originally referred to as the unidentified infrared bands. Evidence for the attribution of PAHs as the carriers of these spectroscopic features is provided by comparison of the astronomical spectra with laboratory and theoretical spectra for a range of PAH species. Of the observations in the various wavelength regimes, the evidence for PAHs as carriers is perhaps most compelling for the IR bands (see, e.g., Allamandola et al. 1989; Tielens 2008 for reviews).

Some 30 yr ago, the IR emission features, which were discovered about a decade earlier and found to be rather constant in the spectra of a large variety of sources, were suggested by several groups to resemble the general IR spectroscopic features of polyaromatic species (Allamandola et al. 1985; Leger & Puget 1984; Sellgren et al. 1983). The main emission features are centered at wavelengths near 3.3, 6.2, 7.7, 8.6, 11.2, and 12.7 μm, although the spectra contain much more detail depending somewhat on the specific source. Based on comparisons with a large body of laboratory and theoretical IR spectra, these features were shown to generally coincide with CH stretching bands (3.3 μm), CC stretching, and in-plane CH bending bands (6–9 μm) and out-of-plane (oop) CH bending bands (11–14 μm) of typical PAH molecules. While databases of theoretical PAH spectra rely mostly on density functional theory (DFT), experimental methods that have been applied to verify these spectra include matrix-isolation spectroscopy (Hudgins et al. 1994; Szczepanski & Vala 1993), absorption spectroscopy of sublimed PAHs (Joblin et al. 1995), cavity-ring down spectroscopy of jet-cooled PAHs (Huneycutt et al. 2004), IR emission spectroscopy using a cryogenically cooled spectrometer (Cook et al. 1996), and various forms of "action spectroscopy" using a combination of tunable IR laser sources and (tandem) mass spectrometers (Knorke et al. 2009; Oomens et al. 2000; Piest et al. 1999; Ricks et al. 2009). To date, these experimental methods have largely addressed neutral and (singly charged) cationic PAHs.

An important observation from these spectra concerns the relative intensities of the bands in the various regions of the IR spectrum varying strongly with the charge state of the molecule. This variation was first reported based on a comparison of the calculated spectra for neutral and cationic anthracene (DeFrees & Miller 1988) and naphthalene (Pauzat et al. 1992) and was confirmed experimentally using matrix-isolated spectroscopy (Szczepanski et al. 1992). It was found to be a general feature of PAH spectra, useful in determining the dominating charge state of PAHs in specific regions of the interstellar medium (Allamandola et al. 1999). The overall appearance of the infrared emission spectrum thus depends strongly on the relative abundances of neutral, positively and negatively charged PAHs (Bakes et al. 2001a, 2001b). The charge state distribution of PAHs has been theoretically modeled in a large number of studies (see, e.g., Dartois & d'Hendecourt 1997; Salama et al. 1996). One of the key parameters determining the charge state distribution is the local ratio of the UV field (G_0) to the electron density (n_e). Conversion of the charge state of PAHs from cationic to neutral and from neutral to anionic occurs as G_0/n_e decreases. Cross-over values for G_0/n_e can be determined from recombination and ionization rates, such that PAHs exist as

cations for $G_0/n_e > 10^4$, as neutrals for values of $G_0/n_e \sim 10^2$–10^3 and primarily as anions at $G_0/n_e \sim 1$ or lower, although these values also depend on PAH size, cloud temperature, and other parameters. Particularly inside dense clouds, where the UV penetration is low, anionic species are believed to dominate. On the other hand, anionic species may also occur in diffuse clouds (Dartois & d'Hendecourt 1997), particularly if the metallicity is sufficiently high, leading to an increased n_e due to more facile UV ionization (Cox & Spaans 2006). Depending on the H-atom density relative to the PAH density, PAHs may even be the dominant negative charge carriers in such clouds (Lepp & Dalgarno 1988) and have pronounced influence on the chemistry of the cloud (Wakelam & Herbst 2008).

The study by Bakes et al. (2001a, 2001b) relies strongly on the relative band intensities in the various regions of the IR spectrum and how they change for PAHs in different charge states, where typical PAH spectra were derived from computations. Based on comparison with experimental data, calculated relative band intensities are known to be fairly accurate for neutral and cationic PAHs. However, few experimental studies have reported spectroscopic data for anionic PAHs. Obtaining data on anionic PAHs using matrix-isolation spectroscopy is particularly cumbersome typically involving the subtraction of spectra recorded under different matrix conditions. Some experimental spectra on radical anion PAHs have however been reported (Wang et al. 2005; Weisman et al. 2005). Gas-phase studies on anionic PAH systems are limited in number and do not address isolated PAH species; IR spectra of hydrated naphthalene cluster anions (Knurr et al. 2012) and the photodissociation spectra of cluster anions of benzene and water (Maeyama et al. 1997) are some of the very few examples.

One of the main obstacles impeding experimental spectra of negatively charged PAHs to be acquired is the relatively low electron affinity (EA) of neutral PAHs (Betowski et al. 2006; Burrow et al. 1987; Denifl et al. 2005; Malloci et al. 2011, 2005; Modelli et al. 2006; Rienstra Kiracofe et al. 2001; Song et al. 2003), typically less than 1 eV for PAHs in the size range up to coronene. Hence, their radical anions ($PAH^{\bullet -}$) are rather unstable under conditions prevailing in instruments used for matrix-isolation spectroscopy or mass-spectrometry based action spectroscopy. In contrast, deprotonated PAHs ($[PAH - H]^-$), i.e. PAH anions missing one hydrogen atom, can be relatively stable as the EA of the aryl radical is usually significantly higher than that of the corresponding arene molecule, as was recently shown in calculations by (Hammonds et al. 2010) and will also be shown below. The increased EA may also enhance their abundance in dense clouds relative to radical anion PAHs (Demarais et al. 2012), which have been considered to be important in the chemical networks of such cold clouds (Lepp & Dalgarno 1988; Wakelam & Herbst 2008).

Here we present experimental IR spectra of a series of deprotonated PAHs (naphthalene, anthracene, and pyrene), constituting the first gas-phase spectra of negatively charged isolated PAHs. The spectra are obtained using a Fourier transform ion cyclotron resonance mass spectrometer (FTICR MS) in combination with free-electron and optical parametric oscillator (OPO) laser sources, thus covering the astrophysically most relevant spectral range from 3 to 16 μm. Experimental spectra are compared to computed spectra and spectra of PAHs in different charge states, paying special attention to relative band intensities.

Please note the nomenclature used: from the closed-shell neutral PAH, also referred to as arene, the addition or removal of an electron gives the odd-electron ionic species referred to as radical anion ($PAH^{-\bullet}$) and radical cation ($PAH^{+\bullet}$), respectively. The addition or removal of a proton on the other hand yields the iso-electronic even-electron protonated ($[PAH+H]^+$) and deprotonated ($[PAH - H]^-$) species. The latter is the main subject of investigation in this study and is also referred to as the aryl anion or the carbanion.

2. EXPERIMENTAL SECTION

2.1. Experiment

Experiments are carried out in the FTICR MS (Marshall et al. 1998), described previously (Polfer & Oomens 2007; Valle et al. 2005) coupled to the beam line of the free-electron laser for infrared experiments (FELIX; Oepts et al. 1995; Polfer & Oomens 2007). The same FTICR MS is also used in combination with a pulsed Nd:YAG pumped OPO (LaserVision, Bellevue, WA) to access the 3 μm wavelength range.

Deprotonated PAHs are generated and stored in the Penning trap of the FTICR MS as outlined in Figure 1(a.) Briefly, the carboxylate anions of the PAH under investigation are generated by electrospray ionization (ESI) of a solution containing the corresponding PAH carboxylic acid, in particular naphthoic acid, anthroic acid, and pyrene carboxylic acid, which were obtained from Tokyo Chemical Industry and used without further purification. Solutions were prepared in a 9:1 methanol:water mixture containing 0.5 mM of the PAH carboxylic acid and about 0.1 mM NH_4OH to enhance deprotonation and hence the formation of PAH carboxylate anions in the ESI process. The carboxylate anions are accumulated in a linear hexapole ion trap and then transferred into the iron cycloton resonance (ICR) cell via an octopole rf ion guide. Sustained off-resonance irradiation collision induced dissociation (SORI-CID; Marshall et al. 1998) of the carboxylate anions induces loss of CO_2 thereby generating the deprotonated $[PAH - H]^-$ species of interest. A stored-waveform inverse Fourier transform (Marshall et al. 1998) excitation pulse is then used to mass-isolate the $[PAH - H]^-$. For the naphthyl ($C_{10}H_7^-$) and anthracenyl ($C_{14}H_9^-$) anions, proton transfer was investigated using two different PAH carboxylic acid isomers as precursor.

The mass-selected $[PAH - H]^-$ carbanions are irradiated with the tunable IR light from FELIX in the 6–16 μm wavelength range (~35 mJ pulse energy, ~5 μs pulse duration, ~0.5% bandwidth). The FELIX wavelength is calibrated with a precision of 0.02 μm using a grating spectrometer, corresponding to a maximum error of ± 5 cm^{-1} over the wavelength range. Spectra over the 3.1–3.6 μm wavelength range are recorded using a pulsed OPO (10 mJ pulse energy, ~6 ns pulse duration, ~3 cm^{-1} bandwidth), which is wavelength calibrated with a precision of ± 1 cm^{-1} using a wavemeter. Whenever the frequency of the laser is in resonance with an IR allowed vibrational mode of the anion, infrared multiple-photon absorption occurs leading to electron detachment from the anion. A spectrum is then obtained by monitoring the depletion of the parent ion as a function of IR frequency. To this end, a series of mass spectra is recorded as the frequency of the laser is tuned. The mass of the naphthyl anion ($C_{10}H_7^-$) is 127 u, of the anthracenyl anion ($C_{14}H_9^-$) is 177 u, and of the pyrenyl anion ($C_{16}H_9^-$) is 201 u.

2.2. Computational

Calculations have been performed at the DFT level using the B3LYP functional and the 6–31++G(d, p) basis set as implemented in Gaussian03. Electronic energies were corrected for

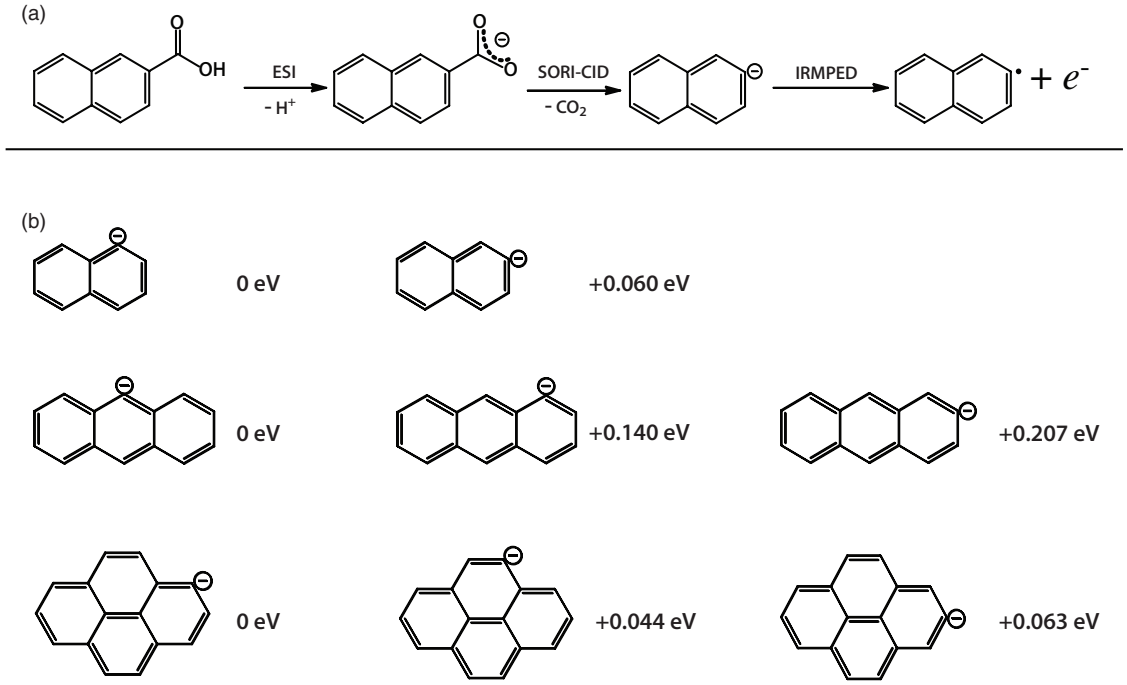

Figure 1. (a) Schematic showing the generation of the 2-naphthyl anion from its 2-naphthoic acid precursor. IR multiple-photon induced electron detachment (IRMPED) is used to detect light absorption as function of the IR wavelength applied (see text for details). (b) Isomeric structures of deprotonated naphthalene, anthracene, and pyrene. Relative energies with respect to the lowest-energy singlet isomer calculated at the B3LYP/6–311+G(*d*, *p*) level of theory are indicated.

zero-point energy (ZPE). Depending on the site of deprotonation, multiple isomers exist for each of the deprotonated PAH species (see Figure 1(b)). For the anions which have been experimentally investigated in this work, geometry optimizations show that (1) for the naphthyl anion, the 2-naphthyl isomer is +0.060 eV higher in electronic energy than the 1-naphthyl anion, (2) for the anthracenyl anion, the 9-anthracenyl isomer is lowest in energy with the 1- and 2-isomers at +0.140 eV and +0.207 eV, respectively, and (3) for the pyrenyl anion, the 1-pyrenyl anion is the most stable isomer, with the 2- and 10-isomers at +0.063 eV and +0.044 eV, respectively.

Transition states (TSs) for proton transfer connecting the different isomers of the aryl anions were computed using the QST3 keyword in Gaussian03. In some cases, a slightly smaller basis set was used to compute the TS, e.g., 6–31+G(*d*, *p*) was employed for the anthracenyl anion. It was verified that the TSs are first-order saddle points and that the normal mode of the imaginary frequency corresponds to the reaction coordinate transferring the proton between the two isomeric positions.

Theoretical vibrational spectra have been computed at the B3LYP/6–31++G(*d*, *p*) level of theory. Harmonic vibrational frequencies in the optimized singlet electronic ground states were calculated ensuring that no imaginary frequencies were present. Calculated vibrational frequencies are scaled by 0.97 in the IR wavelength range between 6 and 16 μm and by 0.957 for wavelengths around 3 μm. These values are in the range of those reported for naphthalene using a similar basis set by (Langhoff 1996). While that paper uses in addition different scaling factors for modes above and below 1300 cm^{-1}, such detailed frequency scaling was not considered useful here given the resolution of the experimental IR multiple-photon induced electron detachment (IRMPED) spectra. For easy comparison of experimental and theoretical spectra, the stick spectra are convoluted with a 15 cm^{-1} FWHM Gaussian lineshape.

Electron affinities were calculated for the dehydrogenated radical [PAH – H]$^\bullet$ systems and compared to those of the corresponding intact even-electron PAH species. To this end, geometry optimizations were carried out for the neutral PAH and [PAH – H]$^\bullet$ systems as well as for their anions. The adiabatic EA is then obtained by subtracting the ZPE corrected minimum energies of the neutral and anion species.

3. RESULTS AND DISCUSSION

3.1. Electron Affinity: Stability of [PAH – H]$^-$ Versus PAH$^{-\bullet}$

Figure 2 shows the adiabatic EAs for a selection of small neutral PAHs (arenes) computed at the B3LYP/6–31++G(*d*, *p*) level of theory. The values obtained here are in good agreement with previous computational and experimental data (see, e.g., Modelli et al. 2006 for a comparison of experimental and computational data). It is seen that the EAs for benzene and naphthalene are predicted to be negative and that the EA generally increases with PAH size, but remains below 1 eV for PAHs up to the size of perylene. The EAs for the series of acenes (anthracene, tetracene, pentacene, etc.) are well-known to be generally higher than the EAs for the more compact PAHs (Modelli et al. 2006), as are the EAs for PAHs comprising one or more five-membered rings (Todorov et al. 2008) and fullerenes. The EA for the compact and highly symmetric coronene molecule ($C_{24}H_{12}$) has been established at about 0.5 eV (Betowski et al. 2006; Carelli & Gianturco 2012; Chen et al. 1996; Denifl et al. 2005; Duncan et al. 1999; Malloci et al. 2005). Although various experimental studies on radical anion PAHs have been reported (Denifl et al. 2005; Duncan et al. 1999), it is anticipated that these species will be unstable under the conditions of our ESI source and Penning trap due to their low EA.

Figure 2 also shows the computed adiabatic EAs for the corresponding aryl radicals, [PAH – H]$^\bullet$, which upon electron attachment form the closed-shell anionic analogs. The adiabatic EAs are calculated as the ZPE corrected difference in electronic energies of the optimized geometries of the neutral radical and

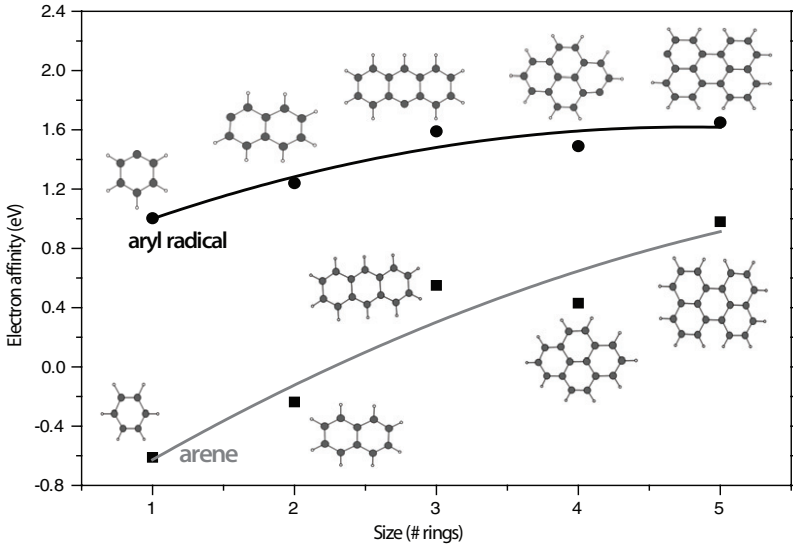

Figure 2. Adiabatic electron affinities for a selection of arene PAHs and aryl radical PAHs computed at the B3LYP/6–31++G(*d*, *p*) level of theory.

Table 1
Band Centers (in cm^{-1}) of the Strongest Bands in the Spectra of the Three Experimentally Studied Deprotonated PAHs

	2-naphthyl Anion			9-anthracenyl Anion			1-pyrenyl Anion		
	Exp.	Calc.	Dev.	Exp.	Calc.	Dev.	Exp.	Calc.	Dev.
	705	705	0	709	709	0	703	698	5
	780	781	−1	789	792	−3	823	825	−2
	1356	1361	−5	987	992	−5	1225	1220	5
				1332	1324	8	1386	1385	1
							1554	1548	6
							1590	1596	−6
rms dev			2.9			4.9			4.6

Notes. Experimental values are compared with computed scaled harmonic frequencies. Bands in the 3 μm range have not been included because of severe spectral congestion.

the singlet anion. It is seen that the EAs for the aryl radicals are substantially higher than those for the corresponding PAH molecules. Deprotonated PAHs ([PAH – H]$^-$) are therefore generally more stable against electron detachment than their corresponding radical anion species (PAH$^{\bullet-}$). The gain in stability amounts to up to more than 1 eV for the smallest PAHs and falls off somewhat toward larger species.

In the following, we present experimental IR spectra for three gas-phase deprotonated PAHs, which are mass-selectively prepared from PAH carboxylic acid precursors using negative ion ESI and CID in a tandem mass spectrometer, as described in the experimental section.

3.2. Infrared Spectra

IRMPED spectra of three PAH anions have been recorded in the 600–1600 cm^{-1} and 2800–3200 cm^{-1} range using 2-naphthoic acid, 9-anthroic acid, and 1-pyrene carboxylic acid as precursors. The spectra of the naphthyl, anthracenyl, and pyrenyl anions (see Figure 1(b)) obtained with these precursors are shown in Figures 3–5, respectively. The two spectral ranges were covered with two different laser systems, FELIX and OPO, which have different pulse structure and pulse duration. It is difficult to accurately assess what the influence of these differences is on the multiple-photon excitation process and hence on the induced electron detachment process, so that it is not possible to directly link the intensities in the two spectral ranges. Center frequencies for the bands in the 6–16 μm range having a relative intensity of more than 25% of the most intense band are listed in Table 1.

The aryl anions formed from the carboxylic acid precursors can exist as distinct isomers depending on the position of the H-atom vacancy on the carbon frame (see Figure 1(b)). For each of the aryl anions studied, these different isomers possess slightly different energies, typically falling within a 0.2 eV range. In order to establish which of these isomers are formed in the SORI-CID (Senko et al. 1994) process, the experimental IR spectra in Figures 3–5 are compared with computed IR spectra for the different isomers for each of the aryl anions.

3.2.1. Naphthyl Anion

Figure 3 compares the naphthyl anion IR spectrum obtained using 2-naphthoic acid as precursor with the computed spectra for the 1-naphthyl and 2-naphthyl anions. It is seen immediately that the spectrum calculated for the 2-naphthyl anion matches the experimental spectrum, while the 1-naphthyl anion computed spectrum provides a poor match. We conclude therefore that despite its higher energy, the 2-naphthyl anion is formed; likely, formation of the higher-energy isomer is a consequence of using the corresponding precursor 2-naphthoic acid.

For the 2-naphthyl anion, the IR-active CH oop bending modes are observed at 705 cm^{-1} and 780 cm^{-1}. The intensity ratio and the position of these bands are in good agreement with the computed IR spectra. Three weaker bands, observable just above the noise level near 1007 cm^{-1}, 1263 cm^{-1}, and 1531 cm^{-1} are in reasonably good agreement with the calculated spectrum and can be attributed to CH in-plane bending and CC stretching modes. The strongest absorption observed at 1356 cm^{-1} corresponds to a blended feature composed of CH in-plane bending and CC stretching modes calculated at 1325 cm^{-1}, 1362 cm^{-1}, and 1394 cm^{-1}. The relative intensity of the band observed at 1356 cm^{-1} is clearly much larger than the sum of its constituents as predicted by the computations. We tentatively attribute this to an often observed artifact in multiple-photon absorption spectra, where closely spaced bands can enhance the IRMPED efficiency. Such effects are obviously not

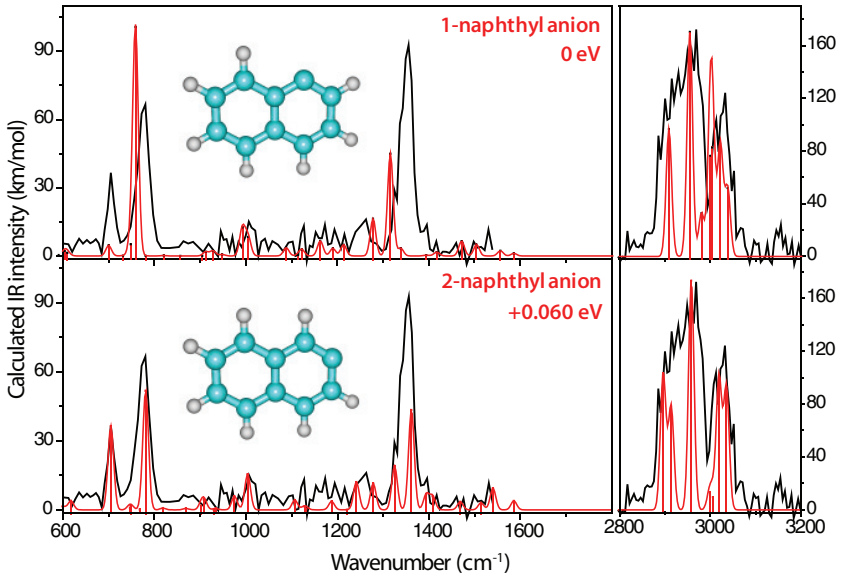

Figure 3. Gas-phase IRMPED spectrum of the naphthyl anion (black) using 2-naphthoic acid as precursor compared to theoretical spectra (red) of singlet 1-naphthyl anion and 2-naphthyl anion. The units of km mol^{-1} refer to the stick spectra only.

(A color version of this figure is available in the online journal.)

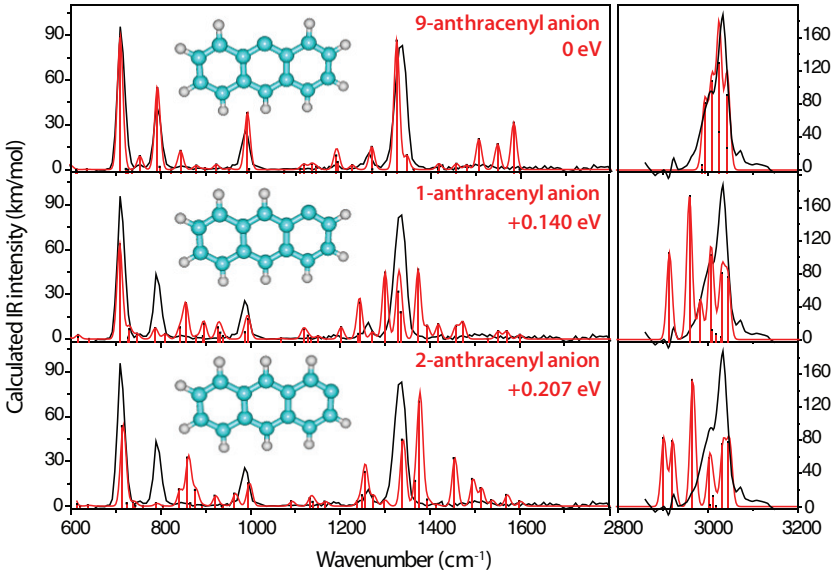

Figure 4. Gas-phase IRMPED spectrum of the anthracenyl anion (black) using 9-anthroic acid as precursor compared to theoretical spectra (red) of the singlet 1-anthracyl, 2-anthracyl and 9-anthracyl anions. The units of km mol^{-1} refer to the stick spectra only.

(A color version of this figure is available in the online journal.)

accounted for in the DFT calculated spectrum, which represents a linear absorption spectrum.

The infrared absorption intensities of PAHs in the 3 μm spectral range are very sensitive to the charge state (Bauschlicher et al. 2009); it is for instance well known that while neutral PAHs possess intense CH stretching bands near 3.3 μm, the corresponding bands in cationic PAHs are about two orders of magnitude weaker. For PAH anions, the CH stretching vibrations are rather intense, as is seen in the calculated spectra of the two naphthyl isomers (Figure 3). For example, in the 2-naphthyl anion, the strongest CH stretching band has a calculated integrated intensity of 173 km mol^{-1}, more than three times higher than that of the CH oop bending mode (52 km mol^{-1}) observed at 780 cm^{-1}.

While the calculated spectrum of the 2-naphthyl anion shows many bands near 3 μm, the experimental spectrum consists of only two relatively broad bands. The discrepancy between observed and calculated spectra can be attributed to a broadening of the bands as a result of the multiple-photon excitation process in the experiment (Oomens et al. 2006). As the molecule becomes energized during the excitation process, absorption bands at frequencies slightly higher than the laser frequency shift into resonance as a consequence of anharmonicity (Parneix et al. 2013). This effect is more pronounced in the CH stretching range because of the high density of vibrational bands and the relatively large anharmonicities (Barker et al. 1987). In addition, the presence of several (weak) overtone and combination bands (Huneycutt et al. 2004) gaining intensity through Fermi and

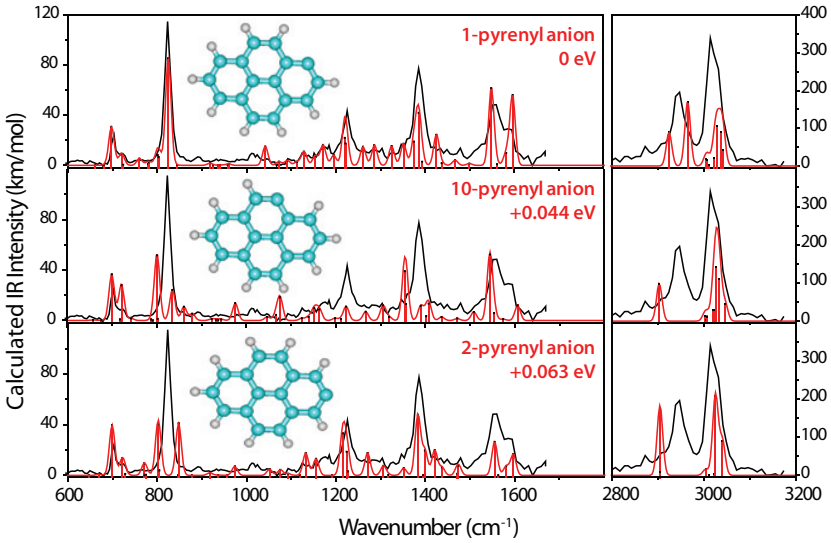

Figure 5. Gas-phase IRMPED spectrum of the pyrenyl anion (black) using 1-pyrene carboxylic acid as precursor compared to theoretical spectra (red) of the singlet 1-pyrenyl, 2-pyrenyl and 10-pyrenyl anions. The units of km mol^{-1} refer to the stick spectra only.
(A color version of this figure is available in the online journal.)

anharmonic resonances with the fundamental bands may add to the spectral congestion observed. Clearly, all of these effects are not accounted for in the DFT calculated spectrum. Nevertheless, convolution of the calculated stick spectrum approaches the experimental spectrum fairly closely for the 2-naphthyl anion, while less convincingly for the 1-naphthyl isomer.

3.2.2. Anthracenyl Anion

In Figure 4, the experimental spectrum of the anthracenyl anion recorded using 9-anthroic acid as precursor is compared with the computed spectra of the 1-anthracenyl, 2-anthracenyl, and 9-anthracenyl anions. Even a superficial glance at the figure establishes that the observed spectrum is due to the 9-isomer of the anthracenyl anion. Hence, as for the naphthyl anion, we find that the anion is deprotonated at the position of the carboxylic acid group in the precursor, which in this case corresponds to the lowest-energy isomer. Judging from the overall comparison of the experimental spectrum with those computed for the 1- and 2-isomers in the upper two panels of Figure 4, it is unlikely that even a small fraction of these isomers is present. This suggests that after dissociation of the PAH carboxylate anion into the aryl anion and a neutral CO_2 molecule, no proton transfer occurs. This hypothesis is further supported by TS calculations presented below.

The CH oop bending features of the 9-anthracenyl anion are observed at 709 cm^{-1} and 789 cm^{-1}. The frequency of CH oop bending modes is known to be dependent on the number of adjacent CH units on an aromatic ring (Allamandola et al. 1989; Hudgins & Allamandola 1999). The 9-anthracenyl anion possesses two aromatic rings with four adjacent hydrogen atoms (referred to as "quartet"); the center aromatic ring has one "solo" hydrogen atom. Animating the calculated normal modes shows that the higher frequency oop band (789 cm^{-1}) corresponds mainly to the solo hydrogen moving, while the lower frequency band (709 cm^{-1}) puts higher vibrational amplitude on the quartet hydrogens. These relative positions of solo and quartet CH oop modes are in agreement with what has been reported for neutral PAHs, although the absolute positions appear to be red-shifted considerably. For neutral PAHs, Hudgins & Allamandola (1999) consider the ranges around 880 cm^{-1} typical for solo CH and around 750 cm^{-1} typical for quartet CH. Upon cationization, these modes typically undergo a blue-shift.

The weaker band located at 987 cm^{-1} is due to a CH in-plane bending mode, while the strongest band in the spectrum near 1332 cm^{-1} is due to CC stretching. Both bands, as well as several weaker bands in the 800–1300 cm^{-1} range are well reproduced by the theory. In contrast, three weaker CC stretching bands predicted at 1507, 1549, and 1585 cm^{-1} are not clearly observed in the experimental IR spectrum, despite several experimental attempts to reveal them. We suspect that a slightly lower laser power in this spectral range, resulting in inefficient multiple-photon excitation, and/or flaws in the computed intensities of these bands are responsible for the deviations.

In the CH stretching range around 3.3 μm, the theoretical IR spectra of the 1- and 2-anthracenyl anion are significantly different from that of the 9-anthracenyl anion. The experimental IR spectrum can therefore be clearly attributed to that of the 9-anthracenyl anion, corroborating the conclusions based on the spectrum observed at longer wavelengths.

3.2.3. Pyrenyl Anion

The spectrum of the pyrenyl anion obtained from the 1-pyrene carboxylic acid precursor is presented in Figure 5. Particularly for the 600–1700 cm^{-1} range, the best agreement with the observed IR spectrum is provided by the computed spectrum of the 1-pyrenyl anion. Hence, we conclude that in analogy with the naphthyl and anthracyl anion, our experimental procedure forms the species deprotonated at the position of the carboxylate group in the precursor. Also in this case, the 1-pyrenyl isomer is slightly lower in energy than the other isomers.

Two main CH oop bending modes are observed at 703 cm^{-1} and 823 cm^{-1} in the experimental spectrum, which agree well with the computed oop bands for the 1-pyrenyl anion, both in position and in relative intensity. Although the 1-pyrenyl anion does not contain any solo hydrogens, the band at 823 cm^{-1} is blue-shifted relative to the oop bands in the experimental IR spectra of the 2-naphthyl (780 cm^{-1}) and 9-anthracenyl (789 cm^{-1}) anions. The relative positions of the bands is still in line with the findings of Hudgins & Allamandola (1999) in the sense that the mode at higher wavenumber has higher

vibrational amplitude on the duo hydrogens, while the mode at 703 cm^{-1} involves larger amplitudes of the trio hydrogens. Nonetheless, the motion of the trio and duo hydrogens are only partially separated and each of the modes involves substantial motion of the alternate set of hydrogen atoms. We suspect that the lower symmetry as a consequence of the missing proton induces substantial mixing between the individual CH oscillators, resulting in deviations from the empirical trends set out in Hudgins & Allamandola (1999).

The bands at 1225 cm^{-1} and 1386 cm^{-1} are recognized as having mainly CH in-plane bending character, although some CC stretching character is mixed in as usual for these modes. The broad feature observed around 1555 cm^{-1} appears to contain at least two sub-features (centered at 1554 and 1590 cm^{-1}), which is supported by the computations: the DFT calculations predict two relatively strong CC stretching modes at 1548 and 1596 cm^{-1}.

The experimental IR spectrum in the CH stretching range shows two strong bands around 2946 cm^{-1} and 3013 cm^{-1}. The agreement with the computed spectrum for the 1-pyrenyl anion is somewhat worse than for the naphthyl and anthracenyl anions. In particular, two computed bands between 2900 and 3000 cm^{-1} are observed as one merged band in the experiment. The observed band at 3013 cm^{-1} appears somewhat stronger than predicted by the calculations. Nevertheless, the computed spectrum for the 1-pyrenyl anion provides a better match to the observed CH stretching bands than the spectra computed for the alternative isomers do.

Table 1 lists experimental band centers in comparison with theoretical ones for each of the attributed isomers. Only bands in the 6–16 μm region with a relative intensity of >25% of the most intense band are included; the 3 μm region is too congested to extract individual band centers. For the strong and well-resolved bands in the table, the rms deviation between experiment and calculation is less than 5 cm^{-1} for the three species studied, which is within the experimental accuracy. This provides confidence in the theoretical method applied here and suggests that it can reliably be used for the calculation of other (larger) deprotonated PAH species. Overall, relative intensities between different wavelength regions are reproduced reasonably well, although individual band intensities may deviate somewhat more. This may be due to experimental artifacts introduced by multiple-photon excitation method or to limitations of the computational method; such deviations are not uncommon.

3.3. Transition States

The spectroscopic findings suggest that no proton transfer occurs after the formation of the aryl anion by loss of a CO_2 unit from the carboxylate precursor. For each of the three systems investigated, the experimental IR spectra identify the deprotonation site as that where the carboxylate group was attached in the precursor. Even when lower-energy isomers are available, as in the case of the 2-naphthyl anion, no evidence for proton transfer was found and the system appears to remain trapped in the higher-energy configuration. Here we use DFT calculations to investigate the barrier to proton transfer in the naphthyl and anthracenyl anions using TS calculations.

The potential energy surface (PES) for proton transfer in the naphthyl anion is sketched in Figure 6. The TS is computed to lie almost 3 eV above the ground state of the two isomers (which differ in energy by only 0.06 eV). While this value is fairly high in itself, it is most important to note that it is significantly above the EA of the naphthyl radical, which is only around 1.2 eV (see Figure 2). This suggests that upon activation, the naphthyl anion detaches its electron well before proton transfer can occur and explains why the alternative isomer cannot be observed in the experimental spectrum.

The PES for the anthracenyl anion shows two TSs for proton transfer between the 1- and 2-isomer and between the 1- and 9-isomer. While the former TS is comparable to that computed for the naphthyl anion, proton transfer between the 1- and 9-positions is computed to be considerably more facile. The transfer of a proton between two adjacent rings apparently faces a lower barrier due to the different TS geometry (see Figure 6). Nonetheless, the approximately 2 eV barrier is still substantially higher than the EA for the anthracenyl radical of about 1.6 eV, again explaining why proton transfer is not observed experimentally.

These theoretical results can be further explored experimentally by recording the spectrum of the aryl anions produced from alternative isomers of the precursor PAH carboxylic acids. IRMPED spectra in the CH stretching range were recorded for the naphthyl anion using 1-naphthoic acid as precursor and for the anthracenyl anion using 2-anthroic acid as precursor. The experimental spectra obtained with the isomeric precursors were clearly found to be different (not shown), suggesting that indeed different deprotonated PAH isomers are formed and that proton scrambling does not occur.

Finally, it is interesting to note the substantial differences in barrier heights with the analogous positive ions, i.e., the carbocation PAHs. Figure 6 shows in addition the computed TS for the 1,2-hydride shift in the naphthyl cation ($C_{10}H_7^+$) in its singlet electronic state. The much lower TS energy (on the order of 1.8 eV compared to 3.0 eV for the anion) is explained based on molecular orbital arguments as being due to the aromatic character of the 3-center 2-electron TS. Experiments on these positively charged species indeed suggested isomerization to occur (Alvaro Galue & Oomens 2011, 2012), although we note that these experiments were carried out under different conditions and moreover, that there is obviously no competition from electron detachment in this case.

3.4. Astrophysical Relevance

The occurrence of negatively charged PAHs in dense regions of the inter- and circumstellar medium has been inferred on the basis of a variety of astronomical observations and theoretical modeling studies. In general, these studies have considered the radical anion PAH species. From the EAs reported here and by others, it is obvious that PAH carbanions (i.e., deprotonated PAHs) are substantially more stable against electron detachment and may therefore be more abundant under astrophysical conditions than radical PAH anions. Anionic PAHs have been suggested to have substantial influence on cloud chemistry (Wakelam & Herbst 2008) and experimental reaction rate constants for PAH carbanions have recently become available (Demarais et al. 2012).

The present study verifies that the IR spectroscopy of PAH carbanions can be reliably predicted using DFT computational methods. Of particular importance in this regard are relative band intensities across the IR spectral range from 3 to 16 μm. Ever since the theoretical studies of DeFrees & Miller (1988) and Pauzat et al. (1992), it is well known that the relative intensities of the bands in the 3 μm (CH stretching), 6–9 μm (CC stretching/CH in-plane bending), and 10–16 μm (CH oop bending) ranges are strongly affected by the charge state of the

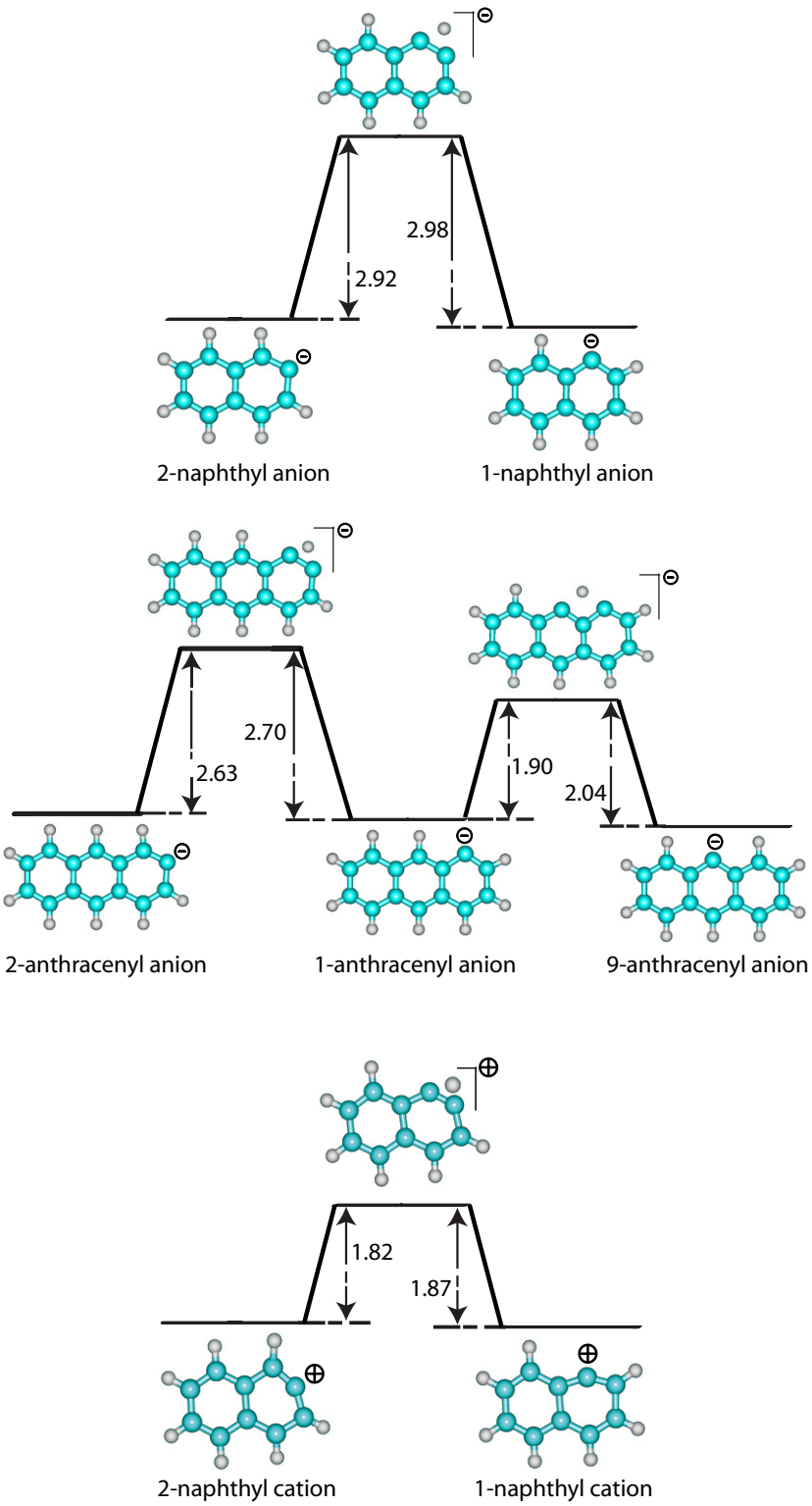

Figure 6. Calculated potential energy surface for proton transfer in the singlet naphthyl (B3LYP/6–31G) and anthracenyl anion (B3LYP/6–31+G(*d*, *p*)) with barrier heights indicated in eV. The potential energy surface for hydride transfer in the cationic counterpart, the singlet naphthyl cation $C_{10}H_7^+$ (B3LYP/6–31+G(*d*, *p*)), is shown for comparison.

(A color version of this figure is available in the online journal.)

PAH. These typical relative band intensities are independent of the specific PAH and can be used as a diagnostic of the charge state distribution and hence as a probe of local interstellar conditions.

With the spectra recorded for the carbanions here, we can now compare relative band intensities for cationic, neutral, and anionic species. To this end, computed IR spectra averaged for a set of small PAHs (anthracene, phenanthrene, pyrene, tetracene, chrysene, and perylene) are shown in Figure 7(a). For the positively charged PAHs, both radical cation and protonated species, representing open- and closed-shell species, respectively, are shown. Laboratory experiments have verified

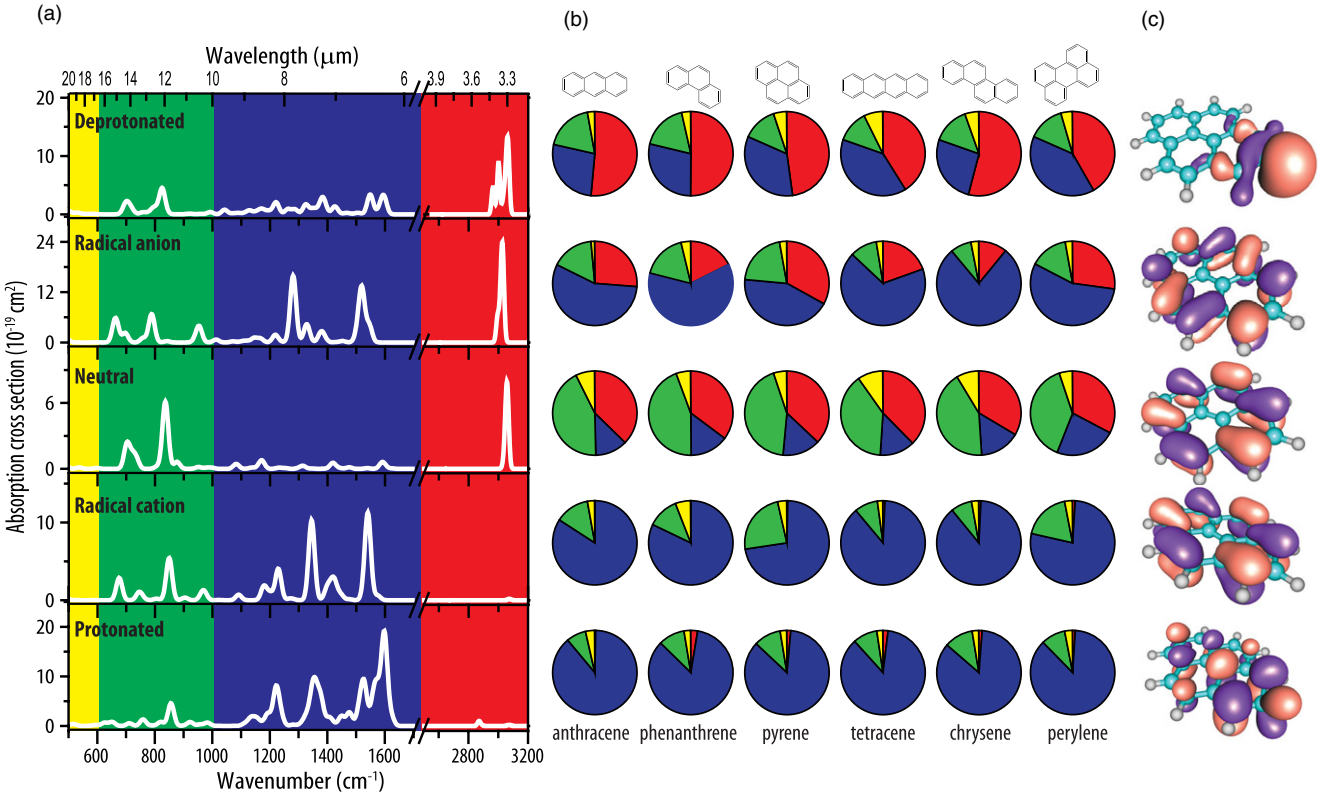

Figure 7. (a) Averaged computed spectra for a set of small PAHs in different charge states. (b) Pie charts indicating for each PAH in the set the relative contribution to the total IR intensity in each of the spectral ranges, color coded as red for 3 μm (CH stretching), blue for 6–10 μm (in plane CC stretching and CH bending), green for 10–16 μm (out-of-plane CH bending) and yellow for >16 μm (skeletal vibrations). (c) Frontier MO carrying the charge for pyrene systems: HOMO for neutral and deprotonated, LUMO for protonated, and SOMO for radical anion and cation. Note that all frontier orbitals are delocalized π-orbitals except for the deprotonated system, where the MO is strongly localized on the deprotonated C-atom and has mainly non-bonding character. (De-)protonation is on the C-atom in position 2, rightmost C-atom in figure.

(A color version of this figure is available in the online journal.)

the general accuracy of the DFT calculated intensities for these species. Also for the negatively charged PAHs, both open-shell (radical anion) and closed-shell (deprotonated) species are included in the analysis. In contrast to neutral PAHs, it is well known that cationic PAHs feature increased intensities for the CC stretching/CH in-plane bending modes (6–9 μm), while their CH stretching bands are reduced in intensity by about two orders of magnitude. Note that computations predict that relative intensities vary substantially with PAH size, so that the CH stretch vibrations of cationic PAHs become of comparable intensity as those of neutral PAHs for sizes around 100 C-atoms (Bauschlicher et al. 2009). For the PAH sizes considered here, the change in relative intensities is roughly similar for both open- and closed-shell cationic PAH species.

In contrast, for the negatively charged PAHs, a more diverging behavior is observed for open versus closed-shell species. Compared with the spectrum for neutral PAHs, both anionic PAH sets feature enhanced intensities in the 6–9 μm range, but the enhancement is about three times larger for the radical PAH anions. Unlike the positive ions, both anionic species have strong absorptions in the 3 μm region, being about two to three times stronger than for the neutral species.

To ensure that the observed trends are general and not due to one specific PAH in the set, Figure 7(b) shows the integrated intensity in four frequency ranges for all members of the set presented as pie charts: red indicates the fraction of the total integrated intensity in the 3 μm range, blue that between 6–10 μm, green that between 10–16 μm, and yellow that at wavelengths longer than 16 μm. Looking along each of the rows, one notices the similarity of the pie charts, indicating that the observed trends are indeed general and not PAH specific. Comparing the different rows, one observes how relative intensities in the open- and closed-shell cations are similar. In contrast, the distribution of intensity over the spectral ranges is rather different for open- and closed-shell anions: relative to the closed-shell deprotonated PAHs, the intensity in the 6–10 μm range increases in the radical anion at the expense of the intensity in the 3 μm range.

The variation of relative band intensities between open- and closed-shell anions in the 6–10 μm range may have implications for the analysis of the interstellar emission band nominally observed at 7.7 μm. Variations in the observed peak position of this band have been suggested to be correlated with the anion/cation ratio (Bregman & Temi 2005): if the band peaks closer to 7.65 μm it is likely carried by cations, while a position closer to 7.85 μm suggests a higher abundance of anions. The spectra for radical cation and anion PAHs in Figure 7(a) nicely illustrate this difference. However, if the anions occur predominantly as deprotonated species, such an analysis may be misguided as neither the computed spectrum for the deprotonated PAHs nor the experimental spectra for the anthracenyl and pyrenyl anions possess a clear band near 7.85 μm ($\sim$1275 cm^{-1}). Note that variations in the intensity of the 7.7 μm band may still be indicative of a change in charge state distribution (Bakes et al. 2001a; Bregman & Temi 2005).

Apart from the differences in relative band intensities, the computed spectra show several interesting shifts in band positions. We do not analyze those in detail here because they depend

sensitively on the DFT functional and scaling factors used, as well as on the limited size range of PAHs in our set. Nonetheless, some interesting qualitative observations are made. As noted before for protonated PAHs (Knorke et al. 2009), deprotonated PAHs also possess CC stretching modes shifted to higher frequencies, closer to the interstellar (nominal) 6.2 μm emission band (Peeters et al. 2002; van Diedenhoven et al. 2004), as compared to the radical anions. Of course, the bands in protonated PAHs have substantially higher absorption cross sections. In the 3 μm range, a more extended band pattern is observed for the deprotonated PAHs as compared to radical anion and neutral PAHs. The position of the CH stretching band has been correlated with the bay or non-bay nature of the CH moieties in the PAH (Bauschlicher et al. 2009; Candian et al. 2012). In general, the CH stretching modes in the anionic systems appear slightly red-shifted ($\sim$30 cm^{-1}) as compared with the neutral PAHs (Bauschlicher et al. 2009). Interstellar emission features indeed show significant red shading of the CH stretching band, although this is usually attributed to anharmonicity (Barker et al. 1987). In the CH oop wavelength region (11–16 μm), where band positions correlate with the number of adjacent H-atoms on an aromatic ring, the bands for the deprotonated PAHs are red-shifted, as discussed in detail in the previous section. The calculated spectra for the radical anion PAHs predict a slightly larger red-shift, whereas these bands are blue-shifted for positively charged PAHs (Hudgins & Allamandola 1999).

In addition to the spectroscopic features, we note the extraordinarily high electric dipole moments for the deprotonated PAHs as revealed by the DFT calculations carried out in this and other recent studies (Hammonds et al. 2010). Regular PAHs have notoriously low dipole moments, usually well below 0.1 D or even zero depending on symmetry. Even in their radical cation or anion forms, the dipole moment is usually low because of charge delocalization over the π-system of the molecule. Breaking the high symmetry of the PAH by adding or removing an H-atom produces a non-zero dipole moment; for instance, the dipole moment for the phenyl radical ($C_6H_5^{\bullet}$) was calculated as 0.9 D and its radiowave spectrum has been recorded (McMahon et al. 2003). Placing a charge on the unsymmetrical PAHs forming (de)protonated systems increases the dipole moment substantially. It is then interesting to note that the dipole moments for the deprotonated (anionic) PAHs are substantially higher than for protonated (cationic) PAHs. For instance, the dipole moment for deprotonated naphthalene is calculated to be 8.2 D versus 2.0 D for protonated naphthalene. For larger deprotonated PAHs, computed dipole moments may even exceed 10 D, such as 11.2 D for phenanthrene, 14.5 D for tetracene, 14.7 D for chrysene, and 9.9 D for coronene (values depending on the site of deprotonation). Note that despite the high permanent dipole moments, detection via radio-astronomy is likely impeded by the small rotational constants, high partition function, large number of ^{13}C-isotopologues, possibly highly heterogenic distribution of PAHs, etc.

The origin of the enhanced dipole moments for deprotonated PAHs is uncovered by inspecting the frontier orbitals in the different charge states, which are shown for pyrene as an example in Figure 7(c). For the radical species, the charge carrier—i.e., the electron for negatively charged systems and the hole for positively charged systems—can be considered to reside in the singly occupied molecular orbital (SOMO); for the cation the SOMO corresponds to the highest occupied MO (HOMO) of the neutral PAH while for the anion it is the lowest unoccupied MO (LUMO) of the neutral PAH, both being delocalized π-orbitals. For the protonated PAH, the positive charge (hole) can be considered to reside in the LUMO, which is also a delocalized π-orbital. In contrast, for the deprotonated PAH, the charge (electron) can be considered to reside in the HOMO, which is a non-bonding *n*-orbital localized on the carbon atom from which the proton is removed. The localized character of this orbital explains the large permanent dipole moment for the deprotonated species. The remarkable difference in relative spectral intensities between the open- and closed-shell anions (Figures 7(a) and (b)) versus the virtually unaltered intensities in open- and closed-shell cations likely also finds its origin in the large variation of the frontier orbitals—and hence charge distributions—of the radical anion and deprotonated species.

4. CONCLUSIONS

The first experimental IR spectra of gaseous negatively charged PAHs have been recorded using a combination of tunable IR lasers (FELIX and OPO) and a tandem mass spectrometer with electrospray source. Even-electron deprotonated PAHs (i.e., PAH carbanions) are formed in the mass spectrometer from PAH carboxylate anions. In general, the experimental spectra for the naphthyl, anthracenyl, and pyrenyl anions compare favorably with their DFT calculated counterparts. The combination of experiment and theory further allows us to estimate the energy for electron detachment and the barrier to proton transfer for these species. Importantly, deprotonated PAHs are more resistant against electron detachment than radical anion PAHs.

Comparison of the IR spectra for deprotonated and radical anion PAHs reveals subtle differences in relative band intensities for the various classes of vibrational modes, whereas these are fairly similar for protonated and radical cation PAHs. Based on an inspection of the frontier orbitals, we conclude that this difference finds its origin in the localized charge in the deprotonated PAH as compared to the charge being delocalized over the π-system in protonated as well as radical anion and cation PAHs. Another manifestation of this charge localization are the extremely high electric dipole moments of deprotonated PAHs.

The experiments performed here are for relatively small PAHs because of the easy commercial availability of the precursor compounds. Further computational investigation is warranted to determine how the observed trends extrapolate to PAH sizes of true interstellar interest, e.g., around 50 C-atoms. It will for instance be of interest to determine whether, and at what PAH size, the difference in EA between open- and closed-shell species vanishes and whether the differences in relative band intensities and dipole moments level off or not. From an experimental standpoint, further study will be required to obtain IR spectra for gas-phase radical anion PAHs.

We gratefully acknowledge the FELIX staff for the skillful technical support. We thank Professor P. J. Sarre and Dr. M. Hammond for stimulating discussions and for sharing their results prior to publication. We thank Professor A. G. G. M. Tielens for numerous discussions and continuing support of our work. This work is sponsored by the Nederlandse Organisatie voor Wetenschappelijk Onderzoek (NWO) Chemical Sciences (CW) as part of the Dutch Astrochemistry Network and under VICI grant No. 724.011.002; it was further supported by NWO Physical Sciences (EW) for the use of the supercomputer facilities at SurfSara. J.O. thanks the Stichting Physica. This work is part of the research program of FOM, which is financially supported by NWO.

REFERENCES

Allamandola, L. J., Hudgins, D. M., & Sandford, S. A. 1999, ApJL, 511, L115
Allamandola, L. J., Tielens, A. G. G. M., & Barker, J. R. 1985, ApJL, 290, L25
Allamandola, L. J., Tielens, A. G. G. M., & Barker, J. R. 1989, ApJS, 71, 733
Alvaro Galue, H., & Oomens, J. 2011, Angew. Chem., Int. Ed., 50, 7004
Alvaro Galue, H., & Oomens, J. 2012, ApJ, 746, 83
Bakes, E. L. O., Tielens, A. G. G. M., & Bauschlicher, C. W., Jr. 2001a, ApJ, 556, 501
Bakes, E. L. O., Tielens, A. G. G. M., Bauschlicher, C. W., Jr., Hudgins, D. M., & Allamandola, L. J. 2001b, ApJ, 560, 261
Barker, J. R., Allamandola, L. J., & Tielens, A. G. G. M. 1987, ApJL, 315, L61
Bauschlicher, C. W., Jr., Peeters, E., & Allamandola, L. J. 2009, ApJ, 697, 311
Betowski, L. D., Enlow, M., Riddick, L., & Aue, D. H. 2006, JPCA, 110, 12927
Bregman, J. D., & Temi, P. 2005, ApJ, 621, 831
Burrow, P. D., Michejda, J. A., & Jordan, K. D. 1987, JChPh, 86, 9
Candian, A., Kerr, T. H., Song, I.-O., McCombie, J., & Sarre, P. J. 2012, MNRAS, 426, 389
Carelli, F., & Gianturco, F. A. 2012, MNRAS, 422, 3643
Chen, G., Cooks, R. G., Corpuz, E., & Scott, L. T. 1996, J. Am. Soc. Mass Spectrom., 7, 619
Cook, D. J., Schlemmer, S., Balucani, N., et al. 1996, Natur, 380, 227
Cox, N. L. J., & Spaans, M. 2006, A&A, 451, 973
Dartois, E., & d'Hendecourt, L. 1997, A&A, 323, 534
DeFrees, D. J., & Miller, M. D. 1988, in Interstellar Dust, The Effect of Ionization on the Infrared Absorption Spectra of PAHs: A Preliminary Report, ed. A. G. G. M. Tielens & L. J. Allamandola (Santa Clara, CA: NASA Conference Publications), 173
Demarais, N. J., Yang, Z., Martinez, O., Jr., et al. 2012, ApJ, 746, 1
Denifl, S., Ptasińska, S., Sonnweber, B., et al. 2005, JChPh, 123, 104308
Duncan, M. A., Knight, A. M., Negishi, Y., et al. 1999, CPL, 309, 49
Hammonds, M., Pathak, A., Candian, A., & Sarre, P. J. 2010, in PAHs and the Universe, Spectroscopy of Protonated and Deprotonated PAHs, ed. C. Joblin & A. G. G. M. Tielens (Toulouse, France: EAS), 373
Hudgins, D. M., & Allamandola, L. J. 1999, ApJL, 516, L41
Hudgins, D. M., Sandford, S. A., & Allamandola, L. J. 1994, JPhCh, 98, 4243
Huneycutt, A. J., Casaes, R. N., McCall, B. J., et al. 2004, Chem. Phys. Chem., 5, 321
Joblin, C., Boissel, P., Leger, A., d'Hendecourt, L., & Defourneau, D. 1995, A&A, 299, 835
Knorke, H., Langer, J., Oomens, J., & Dopfer, O. 2009, ApJL, 706, L66
Knurr, B. J., Adams, C. L., & Weber, J. M. 2012, JChPh, 137, 104303
Langhoff, S. R. 1996, JPhCh, 100, 2819
Leger, A., & Puget, J. L. 1984, A&A, 137, L5
Lepp, S., & Dalgarno, A. 1988, ApJ, 324, 553
Maeyama, T., Oikawa, T., Seguchi, K., & Mikami, N. 1997, JPCA, 101, 8371
Malloci, G., Cappellini, G., Mulas, G., & Mattoni, A. 2011, CP, 384, 19
Malloci, G., Mulas, G., Cappellini, G., Fiorentini, V., & Porceddu, I. 2005, A&A, 432, 585
Marshall, A. G., Hendrickson, C. L., & Jackson, G. S. 1998, Mass Spectrom. Rev., 17, 1
McMahon, R. J., McCarthy, M. C., Gottlieb, C. A., et al. 2003, ApJL, 590, L61
Modelli, A., Mussoni, L., & Fabbri, D. 2006, JPCA, 110, 6482
Oepts, D., Van Der Meer, A. F. G., & Van Amersfoort, P. W. 1995, InPhT, 36, 297
Oomens, J., Sartakov, B. G., Meijer, G., & von Helden, G. 2006, IJMSp, 254, 1
Oomens, J., van Roij, A. J. A., Meijer, G., & von Helden, G. 2000, ApJ, 542, 404
Parneix, P., Basire, M., & Calvo, F. 2013, JPCA, 117, 3954
Pauzat, F., Talbi, D., Miller, M. D., DeFrees, D. J., & Ellinger, Y. 1992, JPhCh, 96, 7882
Peeters, E., Hony, S., Van Kerckhoven, C., et al. 2002, A&A, 390, 1089
Piest, H., von Helden, G., & Meijer, G. 1999, ApJL, 520, L75
Polfer, N. C., & Oomens, J. 2007, PCCP, 9, 3804
Ricks, A. M., Douberly, G. E., & Duncan, M. A. 2009, ApJ, 702, 301
Rienstra Kiracofe, J. C., Barden, C. J., Brown, S. T., & Schaefer, H. F. 2001, JPCA, 105, 524
Salama, F., Bakes, E. L. O., Allamandola, L. J., & Tielens, A. G. G. M. 1996, ApJ, 458, 621
Sellgren, K., Werner, M. W., & Dinerstein, H. L. 1983, ApJL, 271, L13
Senko, M. W., Speir, J. P., & McLafferty, F. W. 1994, AnaCh, 66, 2801
Song, J. K., Lee, N. K., Kim, J. H., Han, S. Y., & Kim, S. K. 2003, JChPh, 119, 3071
Szczepanski, J., Roser, D., Personette, W., et al. 1992, JPhCh, 96, 7876
Szczepanski, J., & Vala, M. 1993, ApJ, 414, 646
Tielens, A. G. G. M. 2008, ARA&A, 46, 289
Todorov, P. D., Koper, C., van Lenthe, J. H., & Jenneskens, L. W. 2008, CPL, 454, 30
Valle, J. J., Eyler, J. R., Oomens, J., et al. 2005, RSciI, 76, 023103
van Diedenhoven, B, Peeters, E., Van Kerckhoven, C., et al. 2004, ApJ, 611, 928
Wakelam, V., & Herbst, E. 2008, ApJ, 680, 371
Wang, H., Szczepanski, J., Hirata, S., & Vala, M. 2005, JPCA, 109, 9737
Weisman, J. L., Mattioda, A., Lee, T. J., et al. 2005, PCCP, 7, 109
Williams, D. A., & Taylor, S. D. 1996, QJRAS, 37, 565